

## Article

# Effect of $Zr_2Al_4C_5$ Content on the Mechanical Properties and Oxidation Behavior of $ZrB_2$ -SiC- $Zr_2Al_4C_5$ Ceramics

Qilong Guo <sup>1,\*</sup>, Liang Hua <sup>1</sup>, Hao Ying <sup>1</sup>, Ronghao Liu <sup>1</sup>, Mei Lin <sup>2</sup>, Leilei Li <sup>1</sup> and Jing Wang <sup>1</sup>

<sup>1</sup> School of Civil Engineering, Northwest Minzu University, Lanzhou 730124, China; 287142749@xbmu.edu.cn (L.L.); 13609327860@126.com (J.W.)

<sup>2</sup> School of Civil Engineering, Lanzhou University of Technology, Lanzhou 730050, China; lzlglinmei@126.com

\* Correspondence: guoqilong8@126.com

**Abstract:**  $ZrB_2$ -SiC- $Zr_2Al_4C_5$  multi-phase ceramics with uniform structure and high density were successfully prepared through the introduction of in situ synthesized  $Zr_2Al_4C_5$  into  $ZrB_2$ -SiC ceramic via SPS at 1800 °C. A systematic analysis and discussion of the experimental results and proposed mechanisms were carried out to demonstrate the composition-dependent sintering properties, mechanical properties and oxidation behavior. The results showed that the in situ synthesized  $Zr_2Al_4C_5$  could be evenly distributed in the  $ZrB_2$ -SiC ceramic matrix and inhibited the growth of  $ZrB_2$  grains, which played a positive role in the sintering densification of the composite ceramics. With increasing  $Zr_2Al_4C_5$  content, the Vickers hardness and Young's modulus of composite ceramics gradually decreased. The fracture toughness showed a trend that first increased and then decreased, and was increased by about 30% compared with  $ZrB_2$ -SiC ceramics. The major phases resulting from the oxidation of samples were  $ZrO_2$ ,  $ZrSiO_4$ , aluminosilicate and  $SiO_2$  glass. With increasing  $Zr_2Al_4C_5$  content, the oxidative weight showed a trend that first increased then decreased; the composite ceramic with 30 vol.%  $Zr_2Al_4C_5$  showed the smallest oxidative weight gain. We believe that the presence of  $Zr_2Al_4C_5$  results in the formation of  $Al_2O_3$  during the oxidation process, subsequently resulting in a lowering of the viscosity of the glassy silica scale, which in turn intensifies the oxidation of the composite ceramics. This would also increase oxygen permeation through the scale, adversely affecting the oxidation resistance of the composites with high  $Zr_2Al_4C_5$  content.



**Citation:** Guo, Q.; Hua, L.; Ying, H.; Liu, R.; Lin, M.; Li, L.; Wang, J. Effect of  $Zr_2Al_4C_5$  Content on the Mechanical Properties and Oxidation Behavior of  $ZrB_2$ -SiC- $Zr_2Al_4C_5$  Ceramics. *Materials* **2023**, *16*, 4495. <https://doi.org/10.3390/ma16124495>

Academic Editors: Maria Isabel Osendi and Woo Taik Lim

Received: 17 May 2023  
Revised: 14 June 2023  
Accepted: 19 June 2023  
Published: 20 June 2023



**Copyright:** © 2023 by the authors. Licensee MDPI, Basel, Switzerland. This article is an open access article distributed under the terms and conditions of the Creative Commons Attribution (CC BY) license (<https://creativecommons.org/licenses/by/4.0/>).

**Keywords:**  $ZrB_2$ -SiC composite ceramics;  $Zr_2Al_4C_5$  layered compound; in situ reactions; mechanical properties; oxidation resistance

## 1. Introduction

Transition-metal borides with strong covalent bond characteristics exhibit extremely high stability, hardness and strength. Among them,  $ZrB_2$  has excellent characteristics such as high melting point, hardness, chemical stability, thermal and electrical conductivity as well as low density, which provide it with good application prospects in the aerospace and nuclear energy industries, and in rapid cutting tools and refractory fields [1–4]. In the past two decades,  $ZrB_2$  has been a research hotspot in the field of ultra-high-temperature ceramics. However, the low fracture toughness of only 2–3  $MPa \cdot m^{1/2}$  [3–5] for  $ZrB_2$  ceramics makes it difficult to work with high strength, representing a significant challenge for its practical application.

Researchers have carried out many works on the improvement of the fracture toughness of  $ZrB_2$  ceramics. The addition of SiC particles into  $ZrB_2$  ceramics not only significantly reduced the sintering temperature, but also greatly improved the fracture toughness and high-temperature oxidation resistance in [5,6]. However, the fracture toughness of  $ZrB_2$ -SiC composite ceramics was still low, at 4–6  $MPa \cdot m^{1/2}$  [5]. Compared with particle toughening, the incorporation of a larger-aspect-ratio phase into the matrix normally improves the defect size tolerance of composite materials and consumes more crack growth energy during

the cracking process of composite materials, making these materials show better fracture toughness. An effective strategy is to replace SiC particles with SiC fibers or whiskers [7], as well as the further addition of toughening phases such as graphite flakes [8], graphene [9], BN [10], carbon nanotubes [11], ZrO<sub>2</sub> fiber [12], and carbon fiber [13]. These toughening phases with relatively large lengths and diameters can greatly inhibit the volume effect of matrix defects and improve the toughness of the materials. Hence, materials with a large length-to-diameter ratio and excellent high-temperature mechanical properties would be optimal for toughening phases in ZrB<sub>2</sub>-SiC composite ceramics. A layered Zr-Al(Si)-C material obtained by simultaneously introducing Al and Si into ZrC [14], such as Zr<sub>2</sub>[Al<sub>3.56</sub>Si<sub>0.44</sub>]C<sub>5</sub> (abbreviated Zr<sub>2</sub>Al<sub>4</sub>C<sub>5</sub>), showed merits such as good oxidation resistance, corrosion resistance and strong damage resistance. Together with its layered grains, high aspect ratio, good high-temperature performance and low theoretical density [15], Zr<sub>2</sub>Al<sub>4</sub>C<sub>5</sub> would be an ideal toughening phase for ZrB<sub>2</sub>-SiC composite ceramics.

In our previous works, we successfully fabricated ZrB<sub>2</sub>-SiC-Zr<sub>2</sub>Al<sub>4</sub>C<sub>5</sub> composite ceramics by spark plasma sintering (SPS) using the mixture of synthesized Zr<sub>2</sub>Al<sub>4</sub>C<sub>5</sub> compound powders, and ZrB<sub>2</sub> and SiC powders [16]. But the Zr<sub>2</sub>Al<sub>4</sub>C<sub>5</sub> compound was not evenly dispersed in the ceramic matrix while the obvious agglomeration occurred, which was not conducive to the improvement of mechanical properties of ZrB<sub>2</sub>-SiC composite ceramics. In addition, ZrB<sub>2</sub>-SiC-Zr<sub>2</sub>Al<sub>4</sub>C<sub>5</sub> composite ceramics were directly fabricated by reactive sintering of Zr, Al, C, B<sub>4</sub>C and Si powders [17], but the uneven dispersion of Zr<sub>2</sub>Al<sub>4</sub>C<sub>5</sub> and the small aspect ratio of generated Zr<sub>2</sub>Al<sub>4</sub>C<sub>5</sub> grains could not significantly improve the fracture toughness of composite ceramics.

In situ reaction sintering technology is an important method for sintering composite ceramics, and can ensure the dispersion uniformity of each forming phase [18–20]. Therefore, in this paper the Zr<sub>2</sub>Al<sub>4</sub>C<sub>5</sub> compounds formed by direct in situ reaction during the sintering process were introduced into ZrB<sub>2</sub>-SiC composite ceramics to achieve ZrB<sub>2</sub>-SiC-Zr<sub>2</sub>Al<sub>4</sub>C<sub>5</sub> composite ceramics with an even dispersion of Zr<sub>2</sub>Al<sub>4</sub>C<sub>5</sub> grains and highly dense microstructure.

This study proves that ZrB<sub>2</sub>-SiC exhibits good oxidation resistance in a relatively wide temperature range [21]. However, when the temperature exceeds 1600 °C or in a low oxygen partial pressure environment, SiC will undergo active oxidation to form gaseous SiO, and the vapor pressure of molten SiO<sub>2</sub> on the surface will also increase significantly, resulting in a rapid decrease in the oxidation resistance of ZrB<sub>2</sub>-SiC ceramics [22]. Therefore, measures such as adjusting the viscosity of the liquid protective layer, optimizing the ZrO<sub>2</sub> skeleton and forming a solid protective layer have been proposed, and efforts have been made to introduce a third component addition phase to improve the oxidation resistance. The improvement of the viscosity of the liquid protective layer can further improve the high-temperature oxidation resistance of composite ceramics. To date, the substances that have been identified to effectively increase the viscosity of the SiO<sub>2</sub> glass phase are mainly Ta-containing compounds, such as Ta<sub>5</sub>Si<sub>3</sub> [23], TaSi<sub>2</sub> [24] and TaB<sub>2</sub> [25], etc. These additives have the same oxidation product, Ta<sub>2</sub>O<sub>5</sub>, which makes the SiO<sub>2</sub> glass phase produce phase separation behavior, thereby increasing the viscosity of the glass phase and increasing the oxidation resistance of ceramics. However, when the temperature exceeds 1500 °C, the addition of Ta has a negative effect on the oxidation resistance of the material to a large extent [26], which is strongly related to the volume expansion of the Ta additive before and after the high-temperature oxidation reaction. Similarly, the addition of AlN compounds to the ZrB<sub>2</sub>-SiC system reduces the viscosity of the SiO<sub>2</sub> glass phase, making it easier for oxygen to diffuse into the protective layer [27], making little contribution to its oxidation resistance, or even deteriorating the performance. Previous research results show that the incorporation of Zr<sub>2</sub>Al<sub>4</sub>C<sub>5</sub> compounds can effectively improve the toughness of ZrB<sub>2</sub>-SiC composite ceramics, but there are few studies on the high-temperature oxidation properties of ZrB<sub>2</sub>-SiC-Zr<sub>2</sub>Al<sub>4</sub>C<sub>5</sub> composite ceramics reported in the literature.

This study systematically investigates, for the first time, the microstructure, mechanical properties and oxidation behavior of ZrB<sub>2</sub>-SiC-Zr<sub>2</sub>Al<sub>4</sub>C<sub>5</sub> composite ceramics with in situ

synthesized  $Zr_2Al_4C_5$ , then further explores the toughening mechanism and oxidation resistance mechanism as well as the relationship between material structure and properties, providing a theoretical basis and technical support for the research of  $ZrB_2$ -SiC-based ultra-high-temperature ceramics.

## 2. Experimental Details

### 2.1. Preparation

The raw materials included:  $ZrB_2$  powder (99.5%, 4.7  $\mu\text{m}$ , Alfa Aesar Co. Ltd., Ward Hill, MA, USA), SiC powder (99.5%, 5.5  $\mu\text{m}$ , Shandong Weifang Huamei Company, Weifang, China), Zr powder (99.9%, 10  $\mu\text{m}$ , Beijing Mengtai Youyan Technology Development Center, Beijing, China), Al powder (purity > 99.99%, 8  $\mu\text{m}$ , Shanghai Chemical Reagents of Chinese Medicine Group, Shanghai, China), C powder (purity > 99.9%, 1  $\mu\text{m}$ , Shanghai Capable Graphite Co. Ltd., Shanghai, China) and Si powder (purity > 99.999%, 16  $\mu\text{m}$ , High Purity Materials Kojundo Chemical Laboratory Co. Ltd., Sakado, Japan).

The designed component of composite ceramics was constant 20 vol.% SiC and a total 80 vol.% of  $ZrB_2$  plus  $Zr_2Al_4C_5$ . The  $Zr_2Al_4C_5$  grains were synthesized by the in situ reaction of Zr, Al and graphite powders (molar ratio is 2:6.2:4.8), and the Si powder (4 wt.%) was added as a sintering additive to stabilize the structure of the  $Zr_2Al_4C_5$  compounds, and is able to replace Al solid solution in  $Zr_2Al_4C_5$  to stabilize the crystal lattice [28].

$ZrB_2$ , SiC, Zr, Al, C and Si were weighed according to the component design, and they were mixed evenly by planetary ball mill (Vario-Planetary Mill, Fritsch Pulverisette 4, Germany) under an argon atmosphere at a speed of 400 r/min, using WC grinding media, with a ball-to-powder weight ratio of 6:1. The mixed powder slurry was dried by rotary evaporator, and then passed through a 60 mesh sieve.

The as-synthesized powders were then loaded into a graphite die with a diameter of 15 mm, and then sintered using an SPS system (model-1050, Sumitomo Coal Mining Co. Ltd., Tokyo, Japan). The temperature was measured by an optical pyrometer focused on the surface of the graphite die. The samples were heated to 600 °C at a rate of 300 °C/min, then further heated at an average heating rate of 100 °C/min to 1800 °C, at which point the temperature was held constant for 3 min. The sample was cooled naturally after the sintering period was over. A uniaxial pressure of 20 MPa and a vacuum atmosphere were applied from the start to the end of the sintering cycle.

The content of  $Zr_2Al_4C_5$  in the complex ceramics was designed as 0 vol.%, 10 vol.%, 20 vol.%, 30 vol.% and 40 vol.%, respectively, hereinafter referred to as ZAC0, ZAC10, ZAC20, ZAC30 and ZAC40.

### 2.2. Characterization and Measurement

The bulk density and open porosity of the ceramic samples were measured through Archimedes's immersion method using water as the immersion medium. The phase compositions were analyzed by X-ray diffraction (XRD) using a Rigaku Ultima III diffractometer. Cu radiation was used and the equipment was operated at 40 KV and 40 mA. The XRD patterns were analyzed using MDI Jade v5.0 software. The microstructures of the polished surfaces and fractures were analyzed by SEM-EDS. Mean grain size was determined through image analysis on SEM micrographs of polished surfaces using a commercial software program (Image-Pro Plus v6.0, Media Cybernetics, Silver Springs, MD, USA).

The Young's moduli (E) of the composites were determined using ultrasonic equipment (Panametrics 5072PR) with a fundamental frequency of 20 MHz, and the hardness and fracture toughness were measured using the Vickers indentation method. The indentation fracture method is an acceptable method for the estimation of the indentation fracture resistance of small ceramic products and components due to its simplicity and applicability to small test samples. The IF method does not represent the true fracture toughness, but it can be useful for describing the trend of changing fracture toughness [29–31]. For the detailed operation and calculation methods please refer to our previous work [32].

The oxidation resistance of the material was characterized by the following two methods:

1. The specimen was cut into a cuboid test block of 0.5 mm × 1.5 mm × 1.5 mm. After washing and drying with an ultrasonic cleaner, the TG curve and DSC curve of the test block were determined using a differential thermal analyzer (TGA, Netzsch, STA449C, Germany) during the heating process; the heating rate during the test process was 10 °C/min, and the atmosphere was air.

2. A cuboid test block with a size of 4 cm × 4 cm × 3 cm was prepared by the same method as in (1), and its surface area was expressed by  $S$  (unit: cm<sup>2</sup>). The initial mass  $M_0$  (unit: mg) of the test block was obtained using a high-precision balance (model: BS210S, Germany). Before oxidation, specimens were cleaned in an ultrasonic bath with alcohol. After they were dried, specimens were placed on a zirconia support with ridges to minimize the contact area and oxidation tests were conducted in an electric furnace (model Nabertherm LHT04, Germany). Specimens were heated at 5 °C/min to different temperatures and held for 30 min in static air. The mass  $M_1$  (unit: mg) of the test block was weighed again after calcination. By Formula (1), the oxidative weight gain  $\Delta M$  per unit area of the test block was calculated.

$$\Delta M = \frac{M_1 - M_0}{S} \quad (1)$$

The phase composition and microstructure of the test block after calcination were observed and analyzed by X-ray diffractometer and scanning electron microscope.

### 3. Results and Discussion

#### 3.1. Phase Composition and Microstructure

The effects of Zr<sub>2</sub>Al<sub>4</sub>C<sub>5</sub> content on the density and open porosity of complex ceramics are listed in Table 1. It can be seen from the table that with the increase of the content of in situ synthesized Zr<sub>2</sub>Al<sub>4</sub>C<sub>5</sub>, the open porosity of the composite ceramics showed a trend of first decreasing and then increasing; when the content was 30 vol.%, the open porosity was the lowest, at only 0.22%. The density of composite ceramics showed a decreasing trend because Zr<sub>2</sub>Al<sub>4</sub>C<sub>5</sub> (4.5 g/cm<sup>3</sup>) [15] has a lower density than ZrB<sub>2</sub> (6.09 g/cm<sup>3</sup>) [5].

**Table 1.** Effects of Zr<sub>2</sub>Al<sub>4</sub>C<sub>5</sub> content on density, open porosity, ZrB<sub>2</sub> grain size and mechanical properties of composite ceramics.

Sample	Density (g/cm <sup>3</sup> )	Open Porosity (%)	ZrB <sub>2</sub> Grain Size (μm)	Vickers Hardness (GPa)	Young's Modulus (GPa)	Fracture Toughness (MPa·m <sup>1/2</sup> )
ZAC0	5.36	0.65	4.7 ± 0.7	17.9 ± 0.2	462 ± 15	4.02 ± 0.30
ZAC10	5.07	0.45	4.2 ± 0.6	17.1 ± 0.2	435 ± 20	4.61 ± 0.33
ZAC20	4.96	0.29	3.9 ± 0.6	16.8 ± 0.2	407 ± 15	5.12 ± 0.29
ZAC30	4.83	0.22	3.3 ± 1.0	16.6 ± 0.4	392 ± 15	5.26 ± 0.32
ZAC40	4.63	0.41	3.7 ± 1.1	15.8 ± 0.4	376 ± 15	4.53 ± 0.30

Figure 1 shows the curve of the displacement of the equipment punch with temperature during the sintering process. As can be seen from the figure, all samples shrank with increasing temperature and tended to be roughly the same, but the temperature at which ZAC30 began to shrink was relatively low, due to the addition of Zr, Al and C powders to react with oxides on the surface of the raw material at lower temperatures to eliminate impurities. At the same time, a partial glass phase was formed, which helped the sintering densification process at high temperatures [33]. In addition, the sample incorporated with Zr<sub>2</sub>Al<sub>4</sub>C<sub>5</sub> began to shrink significantly at about 1400 °C because the liquid phase Al appeared during the in situ synthesized Zr<sub>2</sub>Al<sub>4</sub>C<sub>5</sub> to help atom diffusion and particle rearrangement, and accelerated the sintering of composite ceramics. However, when the incorporation amount exceeded 30 vol.%, the oxide on the surface of the raw

material gradually increased and the loss of Al during the sintering process was large, which affected the sintering performance of the multi-phase ceramic.

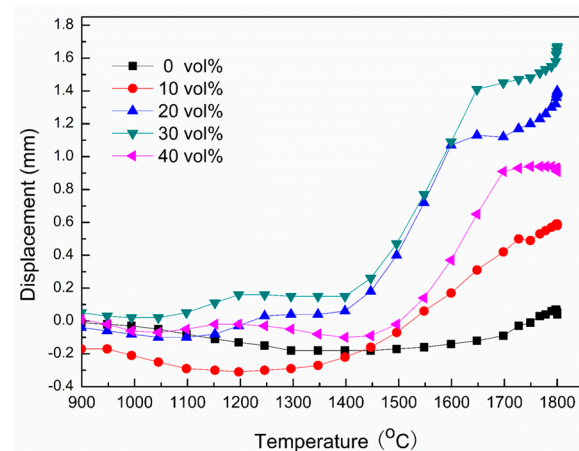


**Figure 1.** Displacement curve of pressure punch at different temperatures.

Figure 2 shows the XRD pattern of  $\text{ZrB}_2\text{-SiC-Zr}_2\text{Al}_4\text{C}_5$  composite ceramics after sintering at 1800 °C for 3 min at different  $\text{Zr}_2\text{Al}_4\text{C}_5$  contents. As can be seen from the figure, diffraction peaks of  $\text{ZrB}_2$  and SiC are present for all specimens. With the increase of the content of in situ synthesized  $\text{Zr}_2\text{Al}_4\text{C}_5$ , the relative intensity of the diffraction peak of  $\text{Zr}_2\text{Al}_4\text{C}_5$  gradually increases. However, when the dosage is 10 vol.%,  $\text{Zr}_3\text{Al}_4\text{C}_6$  compounds appeared because the content of  $\text{Zr}_2\text{Al}_4\text{C}_5$  was small during the sintering process, and it was easily induced by SiC to decompose at high temperatures to form  $\text{Zr}_3\text{Al}_4\text{C}_6$  compounds.

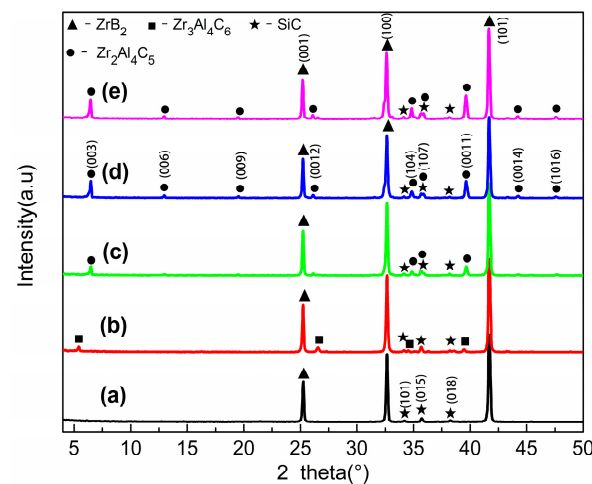


**Figure 2.** XRD patterns of composite ceramics at different  $\text{Zr}_2\text{Al}_4\text{C}_5$  contents: (a) ZAC0, (b) ZAC10, (c) ZAC20, (d) ZAC30, (e) ZAC40.

Figure 3 shows the polished surface of the samples with different  $\text{Zr}_2\text{Al}_4\text{C}_5$  contents' backscattering electron phases. As can be seen from the figure, the black phase is SiC, the gray-white phase is  $\text{ZrB}_2$ , and the dark gray phase is the  $\text{Zr}_2\text{Al}_4\text{C}_5$  layered compound. Compared with the direct incorporation of  $\text{Zr}_2\text{Al}_4\text{C}_5$  layered compounds [15,16], the  $\text{Zr}_2\text{Al}_4\text{C}_5$  compounds generated by in situ reaction could be dispersed in the  $\text{ZrB}_2\text{-SiC}$  ceramic matrix relatively uniformly, and there was no obvious agglomeration. With the increase of  $\text{Zr}_2\text{Al}_4\text{C}_5$  content, the in situ synthesized  $\text{Zr}_2\text{Al}_4\text{C}_5$  layered compounds gradually increased, the length–diameter ratio also gradually increased and the  $\text{ZrB}_2$  grain size gradually decreased. When the content was 30 vol.%, the  $\text{ZrB}_2$  grain size was about 3.3  $\mu\text{m}$  (as shown in

Table 1), which indicated that the in situ reaction to generate  $Zr_2Al_4C_5$  compounds could inhibit the growth of  $ZrB_2$  grains; however, when the content was 40 vol.%, abnormal growth occurred, which was not conducive to the improvement of mechanical properties.

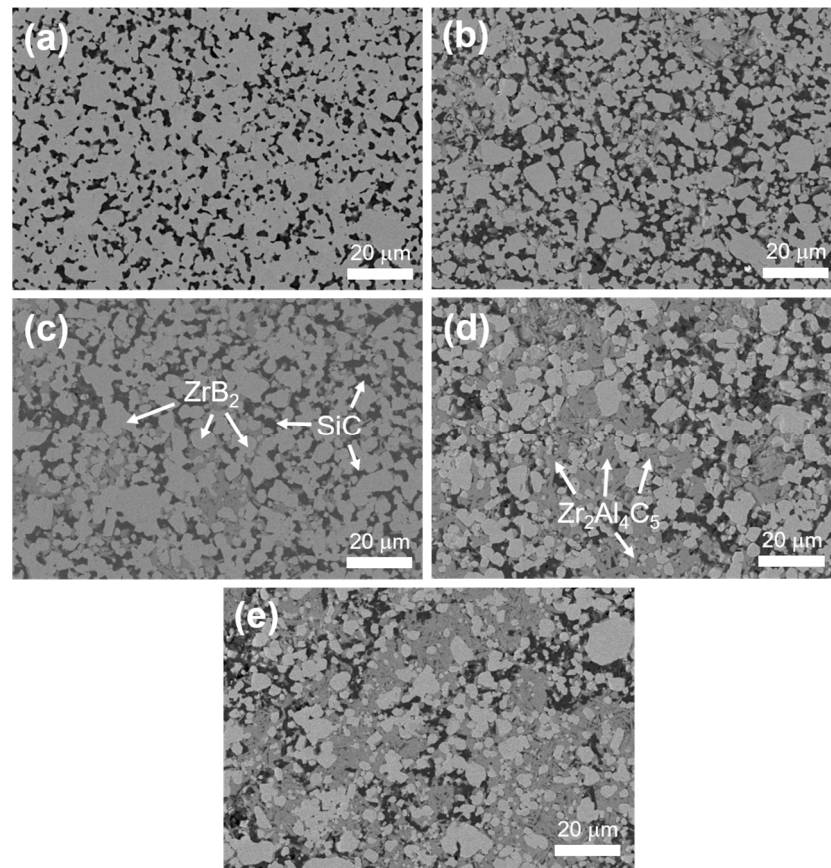


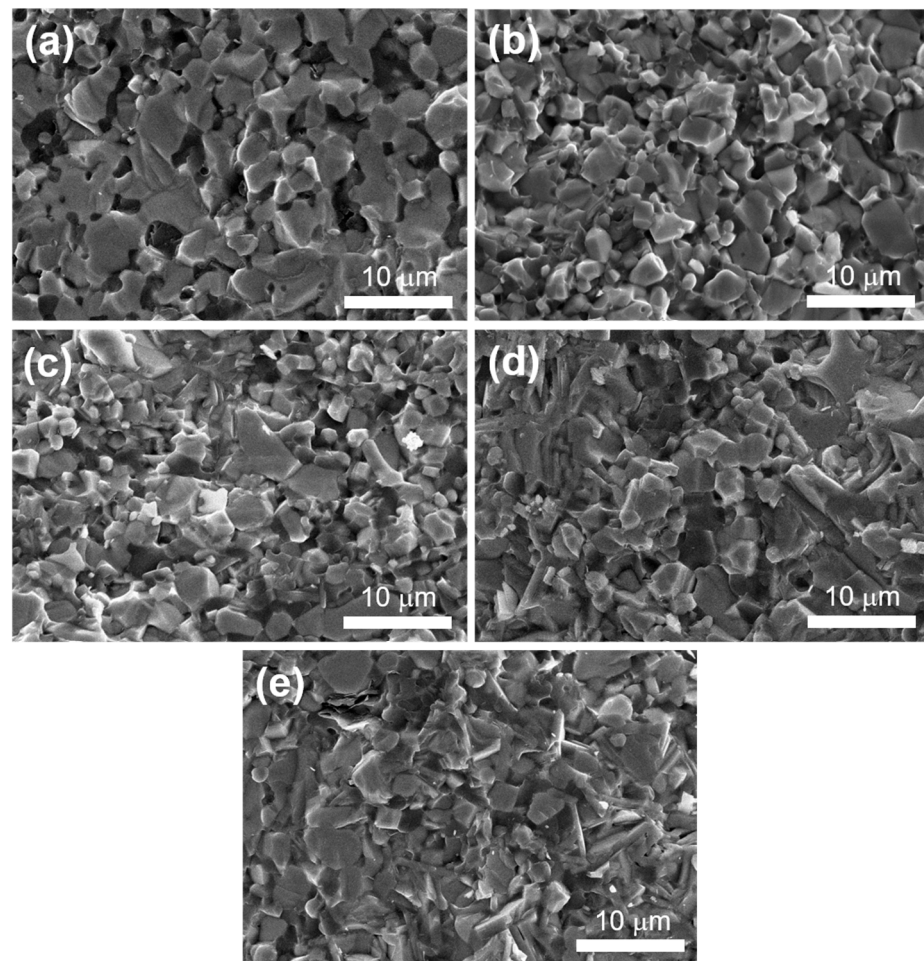
**Figure 3.** Backscattered electron phase pictures of polished surfaces of multi-phase ceramics at different  $Zr_2Al_4C_5$  contents: (a) ZAC0, (b) ZAC10, (c) ZAC20, (d) ZAC30, (e) ZAC40.

### 3.2. Mechanical Properties

The effects of different  $Zr_2Al_4C_5$  contents on the mechanical properties of multi-phase ceramics are summarized in Table 1. It can be seen from the table that with the increase of  $Zr_2Al_4C_5$  content, the Young's modulus and Vickers hardness of the multi-phase ceramics gradually decreased because the Young's modulus and Vickers hardness of  $Zr_2Al_4C_5$  are smaller than those of  $ZrB_2$  [5,15]. With the increase of  $Zr_2Al_4C_5$  content, the fracture toughness first increased and then decreased, and when the dosage was 30 vol.%, its fracture toughness reached a maximum of  $5.26 \text{ MPa} \cdot \text{m}^{1/2}$ , which represents an increase of about 30% compared with  $ZrB_2$ -SiC ceramics, and an increase of nearly 20% compared with that obtained by the direct incorporation of  $Zr_2Al_4C_5$  [16], because the in situ synthesized  $Zr_2Al_4C_5$  compound can be evenly dispersed in the  $ZrB_2$  matrix. Additionally, the length-diameter ratio also increased and the probability of encountering layered structures during crack propagation was also therefore increased, causing more grains to be pulled out or fractured along the crystal and leading to an increase in the crack propagation energy that needs to be consumed. Thereby, the fracture toughness of the material was increased.

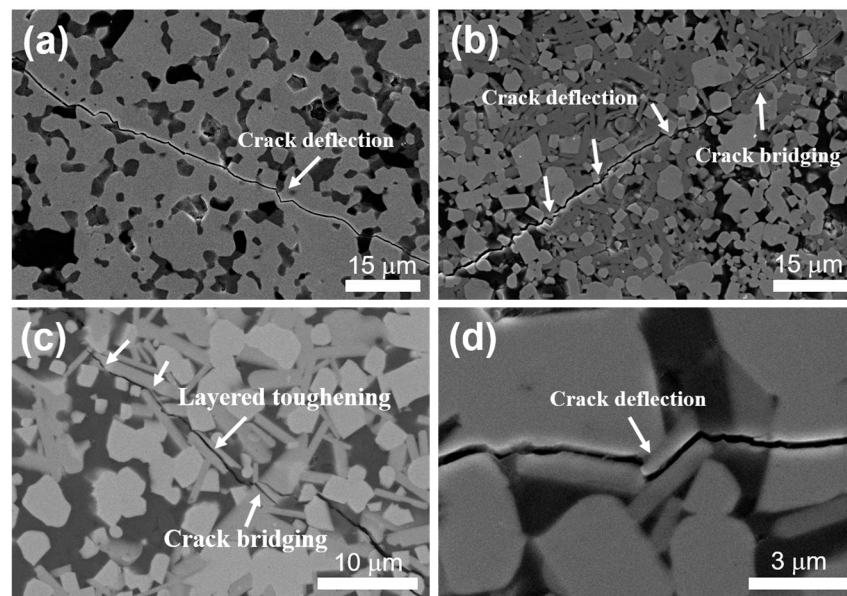
Figure 4 shows the SEM fracture surface morphologies of samples at different  $Zr_2Al_4C_5$  contents. It can be seen the  $ZrB_2$  grain size of the ZAC0 sample was large, as shown in Figure 4a, and the fracture of the complex ceramic was relatively flat. When the  $Zr_2Al_4C_5$  compound was generated by in situ reaction, the fracture of the complex ceramic was rough and dense, and there were traces left by the dialing out of the layered  $Zr_2Al_4C_5$  compound. The fracture mode was presented as a mixed fracture mode of inter- and trans-granular

fractures. With the increase of  $Zr_2Al_4C_5$  content, the roughness degree increased and the grain size of  $ZrB_2$  gradually decreased, as shown in Table 1.



**Figure 4.** SEM fracture surface morphologies of samples with different  $Zr_2Al_4C_5$  content: (a) ZAC0, (b) ZAC10, (c) ZAC20, (d) ZAC30, (e) ZAC40.

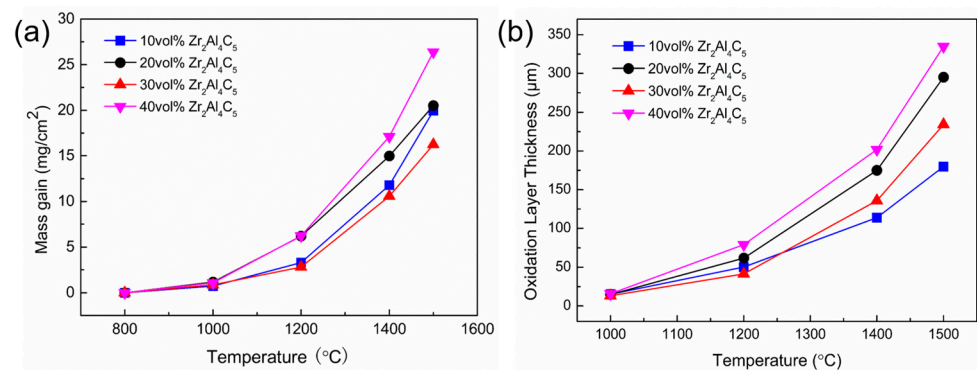
Figure 5 shows the crack tip propagation path diagrams of samples when measuring Vickers hardness. It can be seen that when the  $Zr_2Al_4C_5$  compound was incorporated to change the crack propagation path, there was obvious crack shift and crack bridging (Figure 5b,c). At the same time, when the crack encountered  $Zr_2Al_4C_5$  during the propagation process, the crack repeatedly shifted between its layers and expanded along the weak interface between layers, as shown in Figure 5c, which consumed crack growth energy and improved the fracture toughness of the multi-phase ceramics [34].



**Figure 5.** Expansion path diagram of the crack tip of multi-phase ceramics: (a) ZAC0, (b) ZAC20, (c) ZAC30, (d) ZAC30.

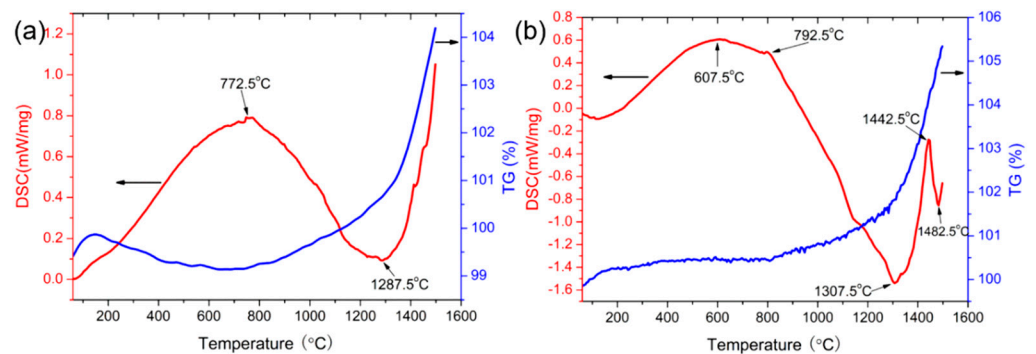
### 3.3. Oxidation Resistance

Figure 6 shows the change of oxidative weight gain and oxide layer thickness of samples under different  $Zr_2Al_4C_5$  contents. It can be seen from the Figure 6 that with the increase of oxidation temperature, the oxidative weight gain and oxide layer thickness of all samples showed a gradually increasing trend; when the temperature was higher than 1200 °C, the oxidative weight gain and oxide layer thickness increase trend was more obvious. With the increase of  $Zr_2Al_4C_5$  content, the oxidative weight gain and oxide layer thickness showed a trend of first increasing, then decreasing and then increasing, and when the dosage was 30 vol.%, the oxidative weight gain was the smallest—16.2 mg/cm<sup>2</sup> at 1500 °C. However, previous research has found that when the content reaches 40 vol.%, the oxidation of complex ceramics is intensified because the  $Zr_2Al_4C_5$  compound is oxidized to generate  $Al_2O_3$  and  $SiO_2$  to form aluminosilicates, which in turn leads to a decrease in the glass phase content of  $SiO_2$ , and the glass phase cannot uniformly cover the surface of the oxide layer, accelerating the diffusion of oxygen to the interior [35]. In addition, more gaseous volatile substances are formed after oxidation, and the evolution of gas causes the oxide layer to form a porous structure, and the  $Al_2O_3$  and  $ZrO_2$  generated by oxidation are dissolved in the glass phase to form a thick and loose oxide layer, which provides many paths for oxygen atoms to enter the inside of the material, causing more serious oxidation.



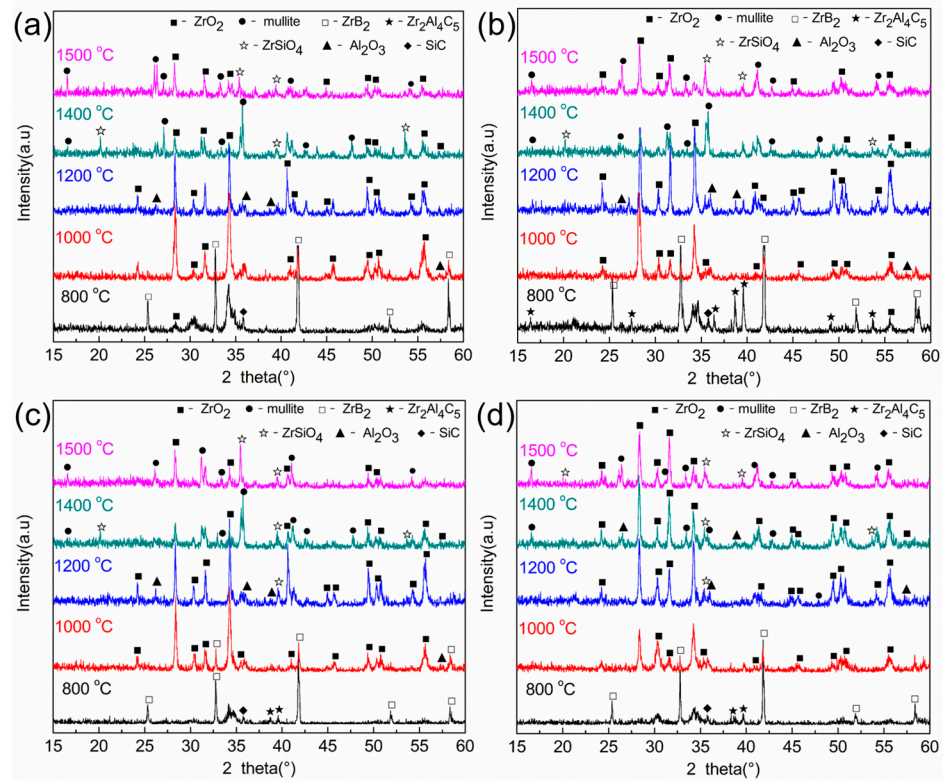
**Figure 6.** (a) Changes of oxidative weight gain and (b) oxidation layer thickness of samples at different contents of  $Zr_2Al_4C_5$ .

Figure 7 shows the thermal stability of ZAC30 and ZAC40 by thermogravimetric (TG) analysis and differential scanning calorimetry (DSC). From the DSC curve, it can be seen that the initial oxidation temperatures of ZAC30 and ZAC40 were 772.5 °C and 607.5 °C, respectively, which indicates that the addition of 30 vol.%  $Zr_2Al_4C_5$  can delay the occurrence of oxidation in the early stage of oxidation. In contrast to the observations of ZAC30, ZAC40 had a significant exothermic peak at 1446.5 °C, which was caused by the reaction of  $SiO_2$  and  $Al_2O_3$  and  $ZrO_2$  by oxidation to form aluminosilicate and  $ZrSiO_4$ . It can be seen from the TG curve that with the increase of oxidation temperature, oxidative weight gain gradually increased, and at temperatures above 1200 °C, the slope of the TG curve increased significantly and the weight gain was obvious.



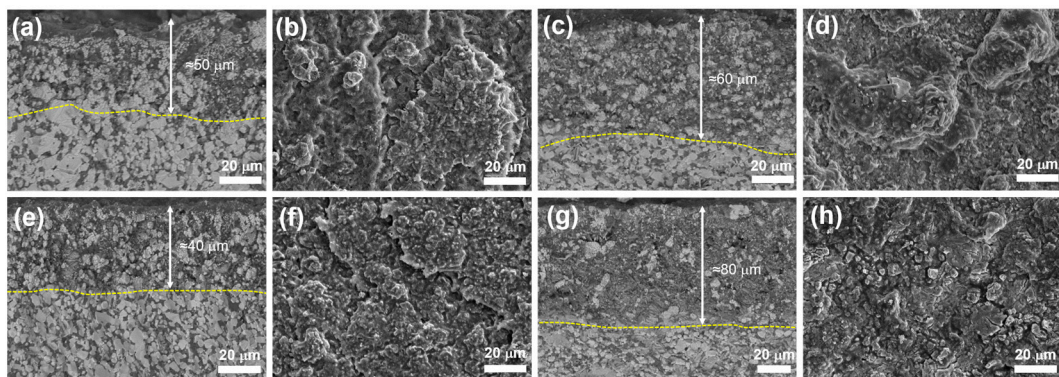
**Figure 7.** TG–DSC curve of multi-phase ceramics: (a) ZAC30, (b) ZAC40. Red line is differential scanning calorimetry, blue line is thermogravimetry.

Figure 8 shows the XRD patterns of the surface layer of the composite ceramic after oxidation for 30 min at different temperatures. The diffraction peaks of  $ZrB_2$ ,  $SiC$  and  $Zr_2Al_4C_5$  compounds could be detected at an oxidation temperature of 800 °C, but there were  $ZrO_2$  diffraction peaks at the same time because  $ZrB_2$  and a small amount of  $Zr_2Al_4C_5$  compounds were oxidized to form  $ZrO_2$  and  $Al_2O_3$  compounds. When the oxidation temperature rose to 1000 °C, the diffraction peak of  $ZrO_2$  gradually strengthened, while the diffraction peak of  $Zr_2Al_4C_5$  was not detected, but the diffraction peak of  $Al_2O_3$  was observed. As the temperature continued to rise, the diffraction peaks of  $ZrO_2$  and  $Al_2O_3$  gradually increased, and when the oxidation temperature reached 1400 °C, the aluminosilicate diffraction peak was significantly enhanced, and with the increase of  $Zr_2Al_4C_5$  content, the diffraction peak gradually weakened. At 1500 °C, the main phases on the surface of the oxide layer were  $ZrSiO_4$ ,  $ZrO_2$  and aluminosilicate, which were due to the reaction of  $SiO_2$  with  $ZrO_2$  to form  $ZrSiO_4$  compounds, and  $SiO_2$  with  $Al_2O_3$  to form aluminosilicates. When the volume content was 30 vol.%, the peak strength of  $ZrSiO_4$  and aluminosilicate diffraction peaks was the strongest.



**Figure 8.** XRD patterns of composite ceramics oxidized for 30 min at different oxidation temperatures: (a) ZAC10, (b) ZAC20, (c) ZAC30, (d) ZAC40.

Figure 9 shows SEM pictures of the cross section and surface of samples after oxidation at 1200 °C for 30 min. It can be seen the oxide layer of the ZAC30 sample was the thinnest, with a thickness of 40 µm, and a thin glassy substance appeared on the surface, which hindered the diffusion of oxygen atoms. However, there were obvious holes in the oxide layer of the ZAC40 sample. It can be seen from the SEM diagram on the surface that the surface of the complex ceramic was uneven and glassy after oxidation, but there were obvious cracks on the surface of ZAC40.



**Figure 9.** SEM pictures of the cross section and surface of the samples after oxidation at 1200 °C for 30 min: (a,b) ZAC10, (c,d) ZAC20, (e,f) ZAC30, (g,h) ZAC40.

Figure 10 shows SEM and EDS pictures of the cross section and surface of the samples after oxidation at 1500 °C for 30 min. It can be seen from the cross-sectional view that the thickness of the oxide layer showed a trend that first increased then decreased with increasing  $Zr_2Al_4C_5$  content; the composite ceramic with 30 vol.%  $Zr_2Al_4C_5$  showed the thinnest oxide layer. When the volume content was 10 vol.%, the oxide layer was the

thinnest, only 170  $\mu\text{m}$ , and the thicker glass phase formed on the surface effectively prevented the diffusion of oxygen atoms. However, when the content increased to 20 vol.%, the glass phase of the surface layer gradually disappeared because the formation of  $\text{Al}_2\text{O}_3$  after oxidation reduced the viscosity of the glass phase and the low-viscosity glass phase also allowed easy penetration of the oxide layer, resulting in no obvious stratification of the oxide layer while the low-viscosity glass phase accelerated the mass transfer process, resulting in the growth of  $\text{ZrO}_2$  grains. When the volume content was increased to 30 vol.%, the oxide layer section had obvious stratification and the oxide layer was thinner, 235  $\mu\text{m}$ , and there was also a thick glass phase on the surface, which effectively prevented oxygen atoms from diffusing into the matrix. When the incorporation amount was 40 vol.%, there was no obvious delamination, the thickness of the glass phase on the surface of the oxide layer progressively decreased, and a large number of holes appeared in the oxide layer, showing a loose porous structure, because with the increase of  $\text{Zr}_2\text{Al}_4\text{C}_5$  content, the content of  $\text{Al}_2\text{O}_3$  generated after oxidation gradually increased, and  $\text{Al}_2\text{O}_3$  and  $\text{SiO}_2$  generated aluminosilicate, resulting in a decrease in the glass phase content of  $\text{SiO}_2$ , which could not be uniformly covered on the surface of the oxide layer. Therefore, only by controlling the appropriate ratio of Al to Si can the oxidation resistance of composite ceramics be optimal because the ratio of Al to Si controls the glass phase viscosity, which can form a dense glass phase protective layer.

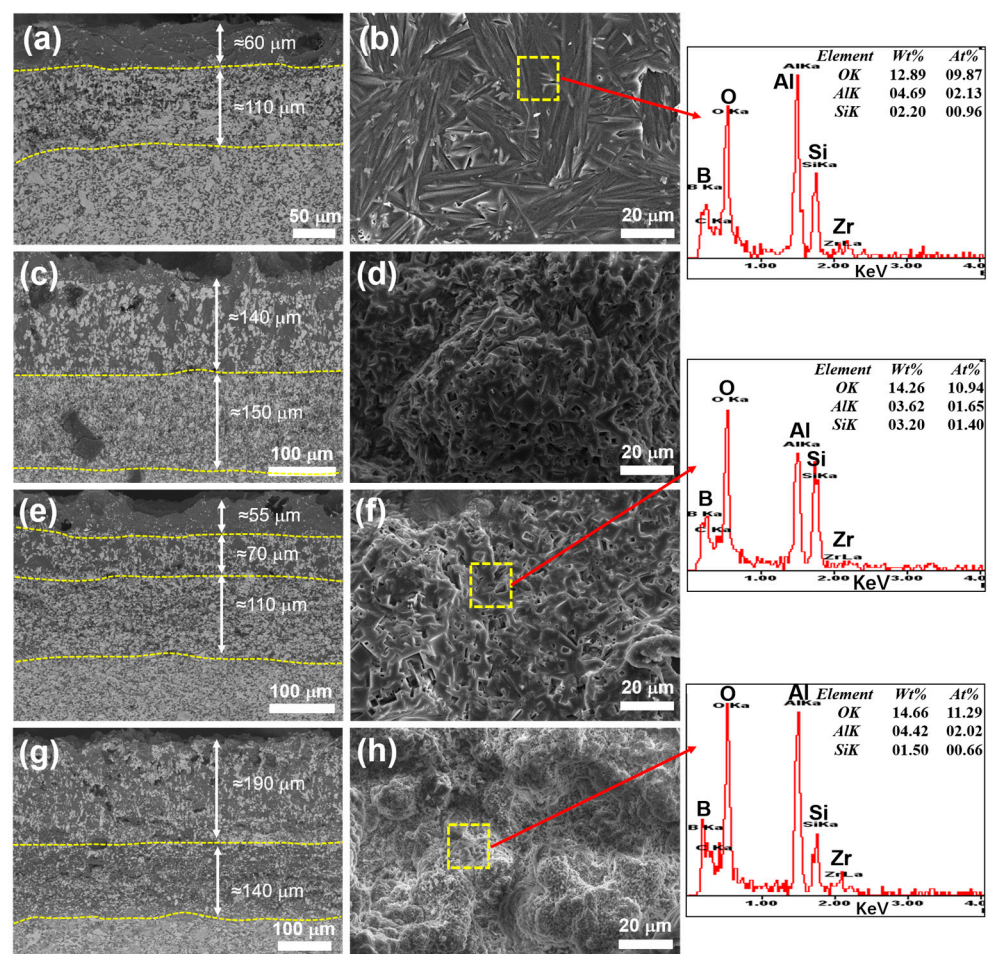


**Figure 10.** SEM and EDS pictures of the cross section and surface of the samples after oxidation at 1200 °C for 30 min: (a,b) ZAC10, (c,d) ZAC20, (e,f) ZAC30, (g,h) ZAC40.

It can be seen from its surface diagram that when the volume content was 10 vol.%, the surface of the oxide layer presented a long strip-like crystalline phase; from the XRD and

EDS analysis it can be seen that these crystals were aluminosilicate and  $Zr_2SiO_4$ . With the increase of  $Zr_2Al_4C_5$  content, the surface of the oxide layer showed obvious unevenness, and the integrity of the surface oxide film was destroyed, indicating that a violent oxidation reaction occurred at this time, generating a large number of volatile gaseous products, which escaped the surface and left holes. Combined with EDS analysis, it can be seen that the main elements on the surface of the oxide layer were silicon, aluminum, oxygen, aluminosilicate and  $SiO_2$  glass phase. With the increase of  $Zr_2Al_4C_5$  volume content, the O content gradually increased.

The distribution of Zr, Al and Si elements can be clearly seen in the cross-sectional element surface scan of the ceramic after oxidation, as shown in Figure 11. It can be seen that when the oxidation temperature was 1200 °C, Al elements gathered on the surface of the oxide layer while silicon elements were present in the lower layer of Al elements. As the diffusivity of Al is greater than the diffusivity of Si, Al more easily diffuses outward at high temperatures [36], and  $Al_2O_3$  formed by oxidation at this temperature is more present in the surface layer of oxidation. When the oxidation temperature was 1400 °C, Si elements began to migrate to the surface of the oxide layer, obvious missing layers of Si and Al elements appeared, and  $Al_2O_3$ ,  $SiO_2$  and aluminosilicate generated after oxidation of the complex ceramics covered the surface of the oxide layer. When the oxidation temperature rose to 1500 °C, the Zr element basically did not appear on the surface of the oxide layer; at this time, due to the high temperature, the Al element on the surface of the oxide layer was also reduced, and the Si element mainly existed on the surface of the oxide layer, so that the surface of the oxide layer was mainly the glass phase of  $SiO_2$  and Al-Si-O, thereby preventing the diffusion of oxygen atoms. Combined with XRD and EDS analysis, the section area after oxidation was divided into four layers: the first layer was the surface of the oxide layer, namely  $SiO_2$ , aluminosilicate and  $Zr_2SiO_4$  and a small amount of  $ZrO_2$ ; the second layer (i.e., the lower layer of the oxide layer) was  $ZrO_2$ ,  $Al_2O_3$ ,  $SiO_2$  and C; the third layer was the missing layer of SiC and  $Zr_2Al_4C_5$  compounds, at which time SiC and  $Zr_2Al_4C_5$  were oxidized to the surface layer at high temperatures (e.g.,  $ZrO_2$ ,  $SiO_2$  and  $Al_2O_3$ ); the fourth layer was the unreacted complex ceramic region.

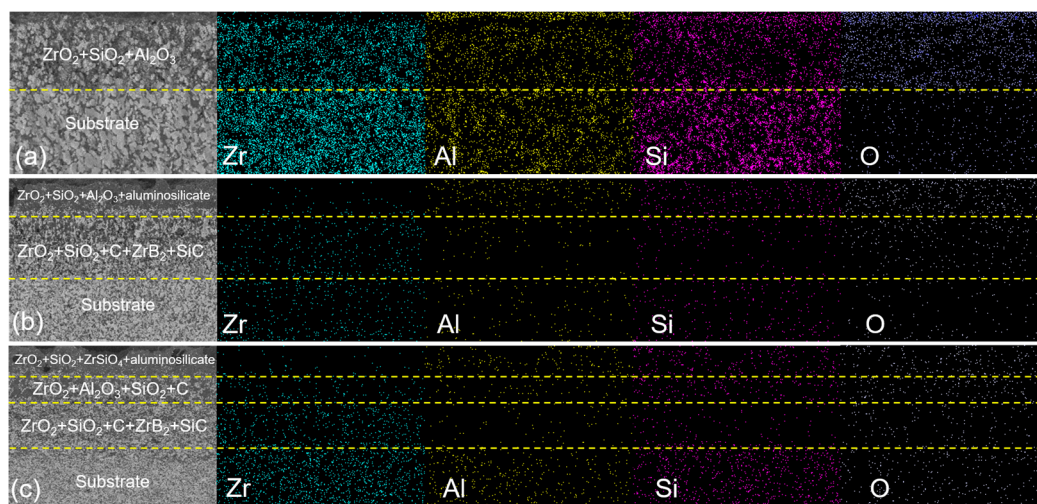


**Figure 11.** EDS pattern of the ZAC30 sample at different oxidation temperatures: (a) 1200 °C, (b) 1400 °C, (c) 1500 °C.

Figure 12 shows a BESEM picture of the ZAC30 sample after 30 min oxidation at 1500 °C. Figure 12b is a local magnification of the second layer area shown in Figure 12a; through EDS analysis, it can be seen that the peaks of Zr, Al and Si appeared at point 1, and the glass phase of Al-Si-O was generated there; the peaks of Si and O at point 3 were more obvious, and the  $SiO_2$  glass phase was generated here; the bright phase was determined to be  $ZrO_2$  by EDS. Through EDS analysis, it was found that the composition

of the glass phase at point 1 and point 3 was different, which was because the diffusivity of Al is greater than that of Si, and Al is more likely to diffuse to the surface layer at high temperature—that is, the surface layer formed a glass phase with a high content of Al-Si-O. Figure 12c shows the area where the third and fourth layers met, and from the enlarged view, it can be seen that the layered Zr-Al-C compounds were the first oxidized, and the layered structure appeared petal-like after oxidation, following the formation of ZrO<sub>2</sub> and Al<sub>2</sub>O<sub>3</sub> compounds.

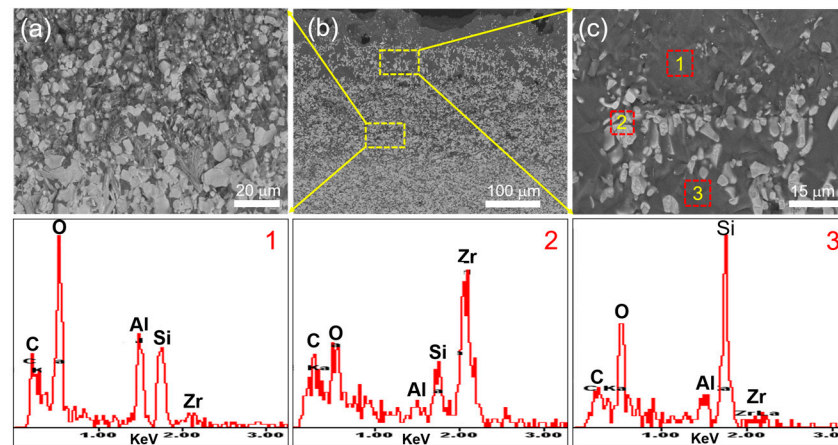


**Figure 12.** BESEM and EDS micrographs of the oxide layer section of the ZAC30 specimen after oxidation at 1500 °C for 30 min (a–c). (a,c) magnified SEM images of the areas enclosed in yellow dotted rectangles in (b).

#### 4. Conclusions

ZrB<sub>2</sub>-SiC-Zr<sub>2</sub>Al<sub>4</sub>C<sub>5</sub> multi-phase ceramics with uniform structure and high density were successfully produced by an in situ reaction sintering process. With the increase of Zr<sub>2</sub>Al<sub>4</sub>C<sub>5</sub> volume content, the open porosity of the composite ceramics showed a trend of first decreasing and then increasing, and when the volume content of the in situ synthesized Zr<sub>2</sub>Al<sub>4</sub>C<sub>5</sub> was 30 vol.%, the porosity of the complex ceramic reached its minimum. Moreover, the grain size of ZrB<sub>2</sub> showed a trend of gradual reduction.

Both the Vickers hardness and Young's modulus of composite ceramics gradually decreased with increasing Zr<sub>2</sub>Al<sub>4</sub>C<sub>5</sub> volume content. The fracture toughness showed a trend of first increasing and then decreasing, and the fracture toughness increased by about 30% compared with that of ZrB<sub>2</sub>/SiC ceramics. It presented as a combination fraction mode of inter- and trans-granular fracture, and there was a phenomenon of pulling out and bridging of layered Zr<sub>2</sub>Al<sub>4</sub>C<sub>5</sub> compounds, which was conducive to the improvement of their fracture toughness.

The oxidative weight gain showed a trend of first increasing and then decreasing and then increasing with an increase in the Zr<sub>2</sub>Al<sub>4</sub>C<sub>5</sub> volume content. When the volume content was 30 vol.%, the oxidative weight gain was the smallest, and there was a thicker glass phase on the surface after oxidation at 1500 °C. However, when the volume content was 20 vol.% and 40 vol.%, the glass phase on the surface of the oxide layer disappeared but obvious holes were present. This is because Zr<sub>2</sub>Al<sub>4</sub>C<sub>5</sub> compounds were oxidized to generate Al<sub>2</sub>O<sub>3</sub> and SiO<sub>2</sub> to form aluminosilicates, which in turn led to a decrease in the content of SiO<sub>2</sub> glass. The glass phase could not uniformly cover the surface of the oxide layer while more gaseous volatile substance was generated, which provided more paths for oxygen atoms to enter the material and intensified the oxidation of the composite ceramics.

Combined with XRD and EDS analysis, the sample after oxidation could be divided into four layers when the volume content was 30 vol.%: the first layer was the surface of the oxide layer, which included SiO<sub>2</sub>, aluminosilicate and Zr<sub>2</sub>SiO<sub>4</sub> and a small amount of ZrO<sub>2</sub>; the second layer was ZrO<sub>2</sub>, Al<sub>2</sub>O<sub>3</sub>, SiO<sub>2</sub> and C; the third layer was the missing layer

of SiC and Zr<sub>2</sub>Al<sub>4</sub>C<sub>5</sub> compounds; and the fourth layer was an unreacted complex ceramic region.

**Author Contributions:** Conceptualization, Q.G.; Validation, M.L., L.L. and J.W.; Investigation, Q.G., M.L., L.L. and J.W.; Writing—original draft, Q.G.; Writing—review & editing, L.H., H.Y. and R.L. All authors have read and agreed to the published version of the manuscript.

**Funding:** This research was funded by the Gansu Provincial Foundation for Science and Technology (20JR5RA510), the Fundamental Research Funds for the Central Universities (31920230178), the National Natural Science Foundation of China (52162011) and the State Key Laboratory of Advanced Technology for Materials Synthesis and Processing (Wuhan University of Technology) (2019-KF-7).

**Data Availability Statement:** Not applicable.

**Acknowledgments:** This work was financially supported by the Gansu Provincial Foundation for Science and Technology (20JR5RA510), the Fundamental Research Funds for the Central Universities (31920230178), the National Natural Science Foundation of China (52162011) and the State Key Laboratory of Advanced Technology for Materials Synthesis and Processing (Wuhan University of Technology) (2019-KF-7).

**Conflicts of Interest:** The authors declare no conflict of interest.

## References

1. Aguirre, T.G.; Lamm, B.W.; Cramer, C.L.; Mitchell, D.J. Zirconium-diboride silicon-carbide composites: A review. *Ceram. Int.* **2022**, *48*, 7344–7361. [[CrossRef](#)]
2. Mohammadzadeh, B.; Jung, S.; Lee, T.H.; Le, Q.V.; Cha, J.H.; Jang, H.W. Manufacturing ZrB<sub>2</sub>-SiC-TaC Composite: Potential Application for Aircraft Wing Assessed by Frequency Analysis through Finite Element Model. *Materials* **2020**, *13*, 2213. [[CrossRef](#)]
3. Fahrenholtz, W.G.; Hilmas, G.E.; Talmy, I.G.; Zaykoski, J.A. Refractory diborides of zirconium and hafnium. *J. Am. Ceram. Soc.* **2007**, *90*, 1347–1364. [[CrossRef](#)]
4. Guo, S.Q. Densification of ZrB<sub>2</sub>-based composites and their mechanical and physical properties: A review. *J. Eur. Ceram. Soc.* **2009**, *29*, 995–1011. [[CrossRef](#)]
5. Asl, M.S.; Nayebi, B.; Ahmadi, Z.; Zamharir, M.J.; Shokouhimehr, M. Effects of carbon additives on the properties of ZrB<sub>2</sub>-based composites: A review. *Ceram. Int.* **2018**, *44*, 7334–7348. [[CrossRef](#)]
6. Zhang, X.H.; Hu, P.; Han, J.C.; Meng, S.H. Ablation behavior of ZrB<sub>2</sub>-SiC ultra high temperature ceramics under simulated atmospheric re-entry conditions. *Compos. Sci. Technol.* **2008**, *68*, 1718–1726. [[CrossRef](#)]
7. Guicciardi, S.; Silvestroni, L.; Nygren, M.; Sciti, D. Microstructure and Toughening Mechanisms in Spark Plasma-sintered ZrB<sub>2</sub> Ceramics Reinforced by SiC Whiskers or SiC-chopped Fibers. *J. Am. Ceram. Soc.* **2010**, *93*, 2384–2391. [[CrossRef](#)]
8. Asl, M.S.; Zamharir, M.J.; Ahmadi, Z.; Parvizi, S. Effects of nano-graphite content on the characteristics of spark plasma sintered ZrB<sub>2</sub>-SiC composites. *Mater. Sci. Eng. A* **2018**, *716*, 99–106.
9. Zhang, X.H.; An, Y.M.; Han, J.C.; Han, W.B.; Zhao, G.D.; Jin, X.X. Graphene nanosheet reinforced ZrB<sub>2</sub>-SiC ceramic composite by thermal reduction of graphene oxide. *Rsc. Adv.* **2015**, *5*, 47060–47065. [[CrossRef](#)]
10. Yue, C.G.; Liu, W.W.; Zhang, L.; Zhang, T.H.; Chen, Y. Fracture toughness and toughening mechanisms in a (ZrB<sub>2</sub>-SiC) composite reinforced with boron nitride nanotubes and boron nitride nanoplatelets. *Scr. Mater.* **2013**, *68*, 579–582. [[CrossRef](#)]
11. Asl, M.S.; Farahbakhsh, I.; Nayebi, B. Characteristics of multi-walled carbon nanotube toughened ZrB<sub>2</sub>-SiC ceramic composite prepared by hot pressing. *Ceram. Int.* **2016**, *42*, 1950–1958.
12. Lin, J.; Zhang, X.H.; Wang, Z.; Han, W.B. Microstructure and mechanical properties of ZrB<sub>2</sub>-SiC-ZrO<sub>2f</sub> ceramic. *Scr. Mater.* **2011**, *64*, 872–875.
13. Sha, J.J.; Li, J.; Lv, Z.Z.; Wang, S.H.; Zhang, Z.F.; Zu, Y.F.; Flauder, S.; Krenkel, W. ZrB<sub>2</sub>-based composites toughened by as-received and heat-treated short carbon fibers. *J. Eur. Ceram. Soc.* **2017**, *37*, 549–558. [[CrossRef](#)]
14. Fukuda, K.; Hisamura, M.; Kawamoto, Y.; Iwata, T. Synthesis, Crystal structure and thermoelectric properties of a new layered carbide (ZrC)<sub>3</sub>[Al<sub>3.56</sub>Si<sub>0.44</sub>]C<sub>3</sub>. *J. Solid. State. Chem.* **2007**, *180*, 1809–1815. [[CrossRef](#)]
15. Zhou, Y.C.; He, L.F.; Lin, Z.J.; Wang, J.Y. Synthesis and structure-property relationships of a new family of layered carbides in Zr-Al(Si)-C and Hf-Al(Si)-C systems. *J. Eur. Ceram. Soc.* **2013**, *33*, 2831–2865. [[CrossRef](#)]
16. Guo, Q.L.; Cao, W.Z.; Gan, J.Z.; Pei, J.J.; Li, J.G.; Zhang, L.M. SPS Fabrication of ZrB<sub>2</sub>-SiC Ceramics Toughened by Zr<sub>2</sub>Al<sub>4</sub>C<sub>5</sub> Compounds and Evaluation of their Properties. *Raer. Metal. Mat. Eng.* **2015**, *44*, 187–191.
17. Guo, Q.L.; Pei, J.J.; Wang, J.; Li, J.G.; Zhang, L.M. Effect of the Content of SiC on Properties of ZrB<sub>2</sub>-SiC-Zr<sub>2</sub>Al<sub>4</sub>C<sub>5</sub> Composite. *Raer. Metal. Mat. Eng.* **2018**, *44*, 282–287.
18. Zhao, Y.; Wang, L.J.; Zhang, G.J.; Jiang, W.; Chen, L.D. Preparation and Microstructure of a ZrB<sub>2</sub>-SiC Composite Fabricated by the Spark Plasma Sintering-Reactive Synthesis (SPS-RS) Method. *J. Am. Ceram. Soc.* **2007**, *90*, 4040–4042. [[CrossRef](#)]
19. Xu, J.Y.; Ma, P.F.; Zou, B.L. Reaction mechanism of ZrB<sub>2</sub>-ZrC formation in Ni-Zr-B<sub>4</sub>C system analyzed by differential scanning calorimetry. *Materials* **2021**, *14*, 6467. [[CrossRef](#)]

20. Rangaraj, L.; Divakar, C.; Jayaram, V. Fabrication and mechanisms of densification of ZrB<sub>2</sub>-based ultra high temperature ceramics by reactive hot pressing. *J. Eur. Ceram. Soc.* **2010**, *30*, 129–138. [[CrossRef](#)]
21. Fahrenholtz, W.G. Thermodynamic analysis of ZrB<sub>2</sub>-SiC oxidation: Formation of a SiC-depleted region. *J. Am. Ceram. Soc.* **2007**, *90*, 143–148. [[CrossRef](#)]
22. Inoue, R.; Arai, Y.; Kubota, Y.; Kogo, Y.; Goto, K. Oxidation of ZrB<sub>2</sub> and its composites: A review. *J. Mater. Sci.* **2018**, *53*, 14885–14906. [[CrossRef](#)]
23. Talmy, I.G.; Zaykoski, J.A.; Opeka, M.M. High-temperature chemistry and oxidation of ZrB<sub>2</sub> ceramics containing SiC, Si<sub>3</sub>N<sub>4</sub>, Ta<sub>5</sub>Si<sub>3</sub>, and TaSi<sub>2</sub>. *J. Am. Ceram. Soc.* **2008**, *91*, 2250–2257. [[CrossRef](#)]
24. Opila, E.; Levine, S.; Lorincz, J. Oxidation of ZrB<sub>2</sub>- and HfB<sub>2</sub>-based ultra-high temperature ceramics: Effect of Ta additions. *J. Mater. Sci.* **2004**, *39*, 5969–5977. [[CrossRef](#)]
25. Peng, F.; Speyer, R.F. Oxidation resistance of fully dense ZrB<sub>2</sub> with SiC, TaB<sub>2</sub>, and TaSi<sub>2</sub> additives. *J. Am. Ceram. Soc.* **2008**, *91*, 1489–1494. [[CrossRef](#)]
26. Silvestroni, L.; Meriggi, G.; Sciti, D. Oxidation behavior of ZrB<sub>2</sub> composites doped with various transition metal silicides. *Corros. Sci.* **2014**, *83*, 281–291. [[CrossRef](#)]
27. Ouyang, G.Y.; Ray, P.K.; Kramer, M.J.; Akinc, M. Effect of AlN substitutions on the oxidation behavior of ZrB<sub>2</sub>-SiC composites at 1600 °C. *J. Am. Ceram. Soc.* **2016**, *99*, 3389–3397. [[CrossRef](#)]
28. Sugiura, K.; Iwata, T.; Yoshida, H.; Hashimoto, S.; Fukuda, K. Syntheses, crystal structures and Si solubilities of new layered carbides Zr<sub>2</sub>Al<sub>4</sub>C<sub>5</sub> and Zr<sub>3</sub>Al<sub>4</sub>C<sub>6</sub>. *J. Solid State Chem.* **2008**, *181*, 2864–2868. [[CrossRef](#)]
29. Miyazaki, H.; Yoshizawa, Y. A reinvestigation of the validity of the indentation fracture (IF) method as applied to ceramics. *J. Eur. Ceram. Soc.* **2017**, *37*, 4437–4441. [[CrossRef](#)]
30. Sktani, Z.D.I.; Rejab, N.A.; Ratnam, M.M.; Ahmad, Z.A. Fabrication of tougher ZTA ceramics with sustainable high hardness through (RSM) optimisation. *Int. J. Refract. Met. Hard Mater.* **2018**, *74*, 78–86. [[CrossRef](#)]
31. Arab, A.; Sktani, Z.D.I.; Zhou, Q.; Ahmad, Z.A.; Chen, P.W. Effect of MgO Addition on the Mechanical and Dynamic Properties of Zirconia Toughened Alumina (ZTA) Ceramics. *Materials* **2019**, *12*, 2440. [[CrossRef](#)] [[PubMed](#)]
32. Guo, Q.L.; Wang, X.Q.; Wang, J. Study on Sintering Processing and Mechanical Properties of In-Situ Reaction-Synthesized Zr<sub>2</sub>Al<sub>4</sub>C<sub>5</sub>-Toughened ZrB<sub>2</sub>-SiC Composite Ceramics. *Mat. Rep.* **2021**, *35*, 06065–06070.
33. Yang, C.; Yao, P.Y.; Huan, Y.; Fu, Z.Q.; Chen, F.; Lavernia, E.J. Tough TiB<sub>2</sub>-based ceramic composites using metallic glass powder as the sintering aid. *Adv. Eng. Mater.* **2016**, *18*, 1936–1943. [[CrossRef](#)]
34. Guo, S.Q. Effects of VC additives on densification and elastic and mechanical properties of hot-pressed ZrB<sub>2</sub>-SiC composites. *J. Mater. Sci.* **2018**, *53*, 4010–4021. [[CrossRef](#)]
35. Guo, Q.L.; Da Silva, C.V.J.; Lin, M.; Luo, S.J.; Pei, J.J.; Wang, X.Q.; Li, J.G.; Zhang, L.M. Influence of composition on microstructure, mechanical properties and oxidation behavior of ZrB<sub>2</sub>/ZrAlC composite ceramics. *J. Ceram. Soc. Jap.* **2019**, *127*, 878–886. [[CrossRef](#)]
36. Yu, L.; Liu, H.; Fu, Y.H.; Hu, W.J.; Wang, Z.F.; Liu, Q.; Wei, B.; Yang, J.; Qiu, T. Design and preparation of an ultra-high temperature ceramic by in-situ introduction of Zr<sub>2</sub>[Al(Si)]<sub>4</sub>C<sub>5</sub> into ZrB<sub>2</sub>-SiC: Investigation on the mechanical properties and oxidation behavior. *J. Adv. Ceram.* **2021**, *10*, 1082–1094. [[CrossRef](#)]

**Disclaimer/Publisher's Note:** The statements, opinions and data contained in all publications are solely those of the individual author(s) and contributor(s) and not of MDPI and/or the editor(s). MDPI and/or the editor(s) disclaim responsibility for any injury to people or property resulting from any ideas, methods, instructions or products referred to in the content.